

Results from the Sudbury Neutrino Observatory

D. Waller for the SNO Collaboration

Ottawa-Carleton Institute for Physics, Department of Physics, Carleton University, Ottawa, Ontario K1S 5B6 Canada

The Sudbury Neutrino Observatory (SNO) has measured the fluxes of electron neutrinos, ν_e , and all flavours of neutrinos, ν_x , from ${}^8\text{B}$ β -decay in the Sun. SNO has determined that $\phi_{\nu_e}/\phi_{\nu_x} = 0.306 \pm 0.026(\text{stat}) \pm 0.024(\text{syst})$. This provides conclusive evidence that most of the ${}^8\text{B}$ ν_e that are produced in the Sun change flavour before they are detected on Earth. This result implies that solar neutrinos have non-zero mass. SNO's measured flux of all active flavour neutrinos, ϕ_{ν_x} , is consistent with the predictions of the Standard Solar Model. Therefore, the smaller than expected flux of solar neutrinos that had been measured by previous solar neutrino experiments can be explained by neutrino flavour change.

1. Introduction

The Sudbury Neutrino Observatory (SNO) is a 1000 tonne heavy water (D_2O) Čerenkov detector located 2 km underground in INCO's Creighton Mine, near Sudbury, Ontario, Canada. The heavy water target in SNO provides three reactions for studying solar neutrinos, each sensitive to different neutrino flavours. SNO can provide unique insight into the nature of neutrinos and can perform a model-independent test of the Standard Solar Model [1].

This paper gives an overview of SNO and its main results so far. Section 2 explains the motivation for building SNO, and Section 3 describes details of the SNO detector. The three solar neutrino reactions that occur in SNO are described in Section 4. SNO's results from the pure D_2O phase of the experiment are summarized in Section 5. The focus of this paper is a description of SNO's most recently published solar neutrino analysis from the "salt phase" of the experiment; these results are presented in Section 6. In addition to SNO's solar neutrino results, two recent non-solar neutrino analyses have been published and are presented in Section 7. The last phase of SNO is briefly outlined in Section 8, and finally, Section 9 contains the conclusion to this paper.

2. Motivation for building SNO

The Sudbury Neutrino Observatory was built to study neutrinos from the β -decay of ${}^8\text{B}$ in the Sun:



By studying these neutrinos, it was hoped that the experiment's ultimate goal could be achieved: solving the Solar Neutrino Problem. Previous solar neutrino experiments measured between 1/2 and 1/3 of the expected flux of solar neutrinos [2–6]; the discrepancy between the previous experimental results and the predictions of the Standard Solar Model [1] is called the Solar Neutrino Problem. For an overview of previous solar neutrino experiments, see Giorgio Gratta's review of neutrino oscillation experiments in these proceedings [7].

There are several possible solutions to the Solar Neutrino Problem:

- all the previous experiments are wrong;
- the predicted solar neutrino fluxes of the Standard Solar Model are wrong;
- solar neutrinos change flavour from ν_e to ν_μ and/or ν_τ ;
- something else happens to the solar neutrinos (e.g. ν_e mix with sterile neutrinos).

Given the large number of measurements by many different experimental collaborations, with many different neutrino detection techniques, the first solution seems unlikely. Many particle physicists favoured the second solution because

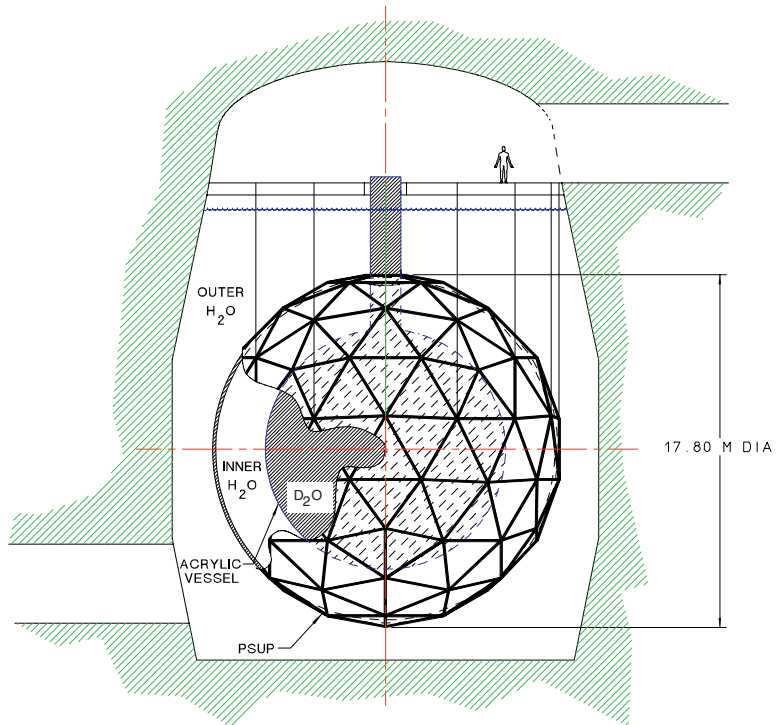


Figure 1: Schematic drawing of the SNO detector. The detector is described in the text.

the Sun is an extremely complex system and the flux of ^8B neutrinos, in particular, is proportional to the Sun's core temperature to the twenty-fifth power! However, the most intriguing possibility, from the particle physics perspective, is that some of the ν_e created in the nuclear reactions in the Sun change flavour before detection at Earth. Solar neutrino experiments before SNO either were sensitive to ν_e only (e.g. the ^{37}Cl and ^{71}Ga radiochemical experiments), or were sensitive mostly to ν_e (e.g. regular water Čerenkov detectors). This means that the lower than expected solar neutrino flux might be elegantly explained by neutrino flavour change. One profound requirement for neutrino flavour change is that solar neutrinos must have non-zero rest mass. For details of the physics of neutrino flavour change, see the lectures of Boris Kayser in these proceedings [8].

Because of SNO's use of heavy water (see Section 4.1), SNO is able to measure both ϕ_{ν_e} , the flux of ν_e , and ϕ_{ν_x} , the flux of all active flavours of neutrinos (ν_e , ν_μ , and ν_τ). If SNO measures a value of ϕ_{ν_e} that is significantly less than ϕ_{ν_x} , then this is direct evidence for neutrino flavour change.

3. The SNO detector

This section gives a brief overview of the SNO detector; for a more detailed description, see [9]. Figure 1 shows an illustration of the SNO detector. SNO's heavy water makes it a unique detector of solar neutrinos; one thousand tonnes of ultra-pure D_2O are contained in a 6 m radius spherical acrylic vessel (AV). The AV is transparent in the visible portion of the electromagnetic spectrum so that Čerenkov photons created after neutrino interactions propagate from the D_2O , through the acrylic, to the photomultipliers (PMTs) that surround the D_2O . There are 9,456 inward-looking PMTs, and 91 outward looking PMTs. The inward-looking PMTs detect photons produced in the inner portion of the detector, while the outward-looking PMTs are used to tag cosmic ray muons that enter the

SNO cavity. The 20 cm diameter PMTs are mounted on a steel support structure (PSUP) that is a geodesic sphere with an 8.9 m radius. In order to increase the geometrical acceptance of the detector, reflective panels are mounted around each PMT; the geometrical acceptance of the PMTs plus reflective panels is 54%. In addition to 1,000 tonnes of D₂O, there are also 7,000 tonnes of ultra-pure H₂O in SNO. The H₂O serves two purposes: it supports the acrylic vessel and D₂O, and it shields the D₂O from natural radioactivity in the PMTs, PSUP, and the rock surrounding the SNO cavity.

All the materials from which the detector was constructed were carefully selected in order to minimize the amount of radioactive backgrounds from elements such as uranium (U) and thorium (Th). Decays of the radioactive daughters of U and Th can produce signals in the SNO detector that are indistinguishable from the signals from solar neutrino interactions. It is especially important to ensure that the D₂O and H₂O have extremely low concentrations of U and Th. The design goal for SNO was to have only a single free neutron per day produced in the detector from natural sources of radioactivity. This translates to 4.5×10^{-14} g/g of U, and 3.7×10^{-15} g/g of Th in the D₂O.

Besides backgrounds from radioactive materials in the detector, another source of background is cosmic rays. SNO is built deep underground to reduce the flux of cosmic ray muons. If SNO were located at the surface, more than a billion cosmic ray muons would pass through it each day. Two kilometres underground, the rate is reduced to 70 per day. Since SNO detects approximately 3,000 solar neutrino interactions per year, the neutrino signal would be swamped by background if SNO were located at or near the Earth's surface.

SNO began taking data in April 1999. The first six months of data were used for commissioning the detector; data taken after commissioning are used for physics analysis. During this first phase of SNO, the acrylic vessel contained only D₂O. The second phase of SNO began in July 2001. At the start of this phase, two tonnes of NaCl were added to the D₂O. The salt was added to improve SNO's neutron detection efficiency. Details of the advantages of adding salt are given in Section 6. This second phase of SNO lasted until August 2003. The salt was then removed by reverse-osmosis, and the detector ran with pure D₂O again for approximately four months. From November 2003 to the present, the detector has been reconfigured and re-commissioned for SNO's final phase. For this phase, ³He proportional counters have been deployed in the D₂O to provide an independent measurement of neutrons. This final phase of SNO is expected to last until the end of 2006.

4. Neutrino interactions in SNO

4.1. SNO's three reactions

The Sudbury Neutrino Observatory is unique because it is able to detect solar neutrinos via three different reactions:



The charged current (CC) reaction, mediated by the charged W boson, on the deuteron, d , is sensitive only to electron neutrinos. The neutral current (NC) reaction, mediated by the neutral Z boson, is equally sensitive to all active flavours of neutrinos. The elastic scattering (ES) reaction is sensitive mostly to electron neutrinos, as $\sigma_{\text{ES}}^{\nu_\mu} = \sigma_{\text{ES}}^{\nu_\tau} \approx 0.15 \sigma_{\text{ES}}^{\nu_e}$. The ES cross-sections for $\nu_{\mu/\tau}$ are smaller than the ES cross-section for ν_e because ν_e can interact with electrons via both Z and W bosons, while $\nu_{\mu/\tau}$ can interact with electrons via Z bosons only. See Figure 2 for Feynman diagrams of the different reactions.

By comparing the flux of electron neutrinos (determined from the measured number of CC reactions) to the flux of all active flavours of neutrinos (determined from the measured number of NC reactions), one can test the hypothesis that all the electron neutrinos produced in the Sun remain electron neutrinos when they reach SNO. If the ratio $\phi_{\text{CC}}/\phi_{\text{NC}}$ is significantly less than one, then there is clear evidence that a fraction of the electron neutrinos are changing flavour to muon or tau neutrinos.

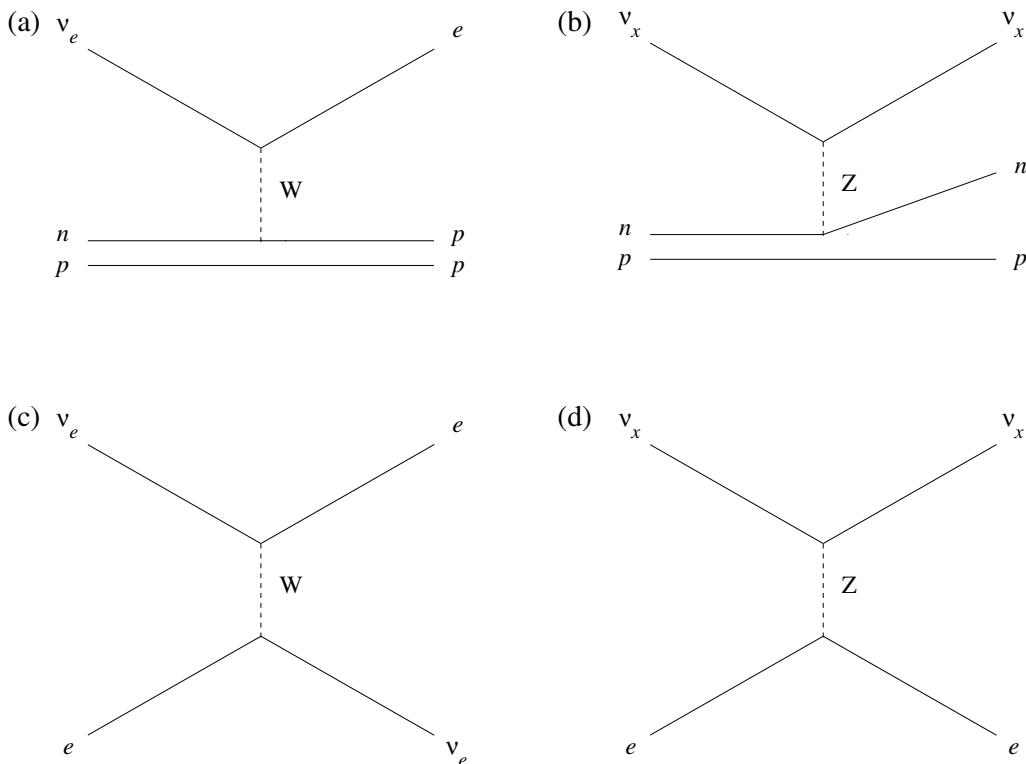


Figure 2: Tree-level Feynman diagrams of the neutrino reactions in SNO. Diagram (a) shows the charged current reaction. Diagram (b) shows the neutral current reaction (resulting in a free neutron). Diagrams (c) and (d) show the graphs that contribute to elastic scattering. Note that only electron neutrinos can scatter from electrons by exchanging a W boson.

If one assumes that all ES reactions are produced by electron neutrinos, a complementary comparison can be made between the electron neutrino flux from ES reactions and the electron neutrino flux from CC reactions. If the electron neutrino flux from ES reactions is significantly greater than the flux from CC reactions, this is evidence that muon and/or tau neutrinos are taking part in ES reactions in the detector. Again, this would provide evidence of electron neutrino flavour change. By comparing the rates of ES, CC and NC reactions, SNO can test the internal consistency of its results.

4.2. Neutrino detection in SNO

All three types of SNO's neutrino reactions are detected by the Čerenkov light that is produced either directly or indirectly. In the CC and ES reactions, a relativistic electron is produced directly. If the velocity of the electron is greater than the speed of light in the D₂O, a cone of Čerenkov radiation is emitted by the electron at a 42° angle with respect to the direction of propagation of the electron. The ring of PMT hits that results from the projection of the Čerenkov cone on the PMT array is the signal for a solar neutrino interaction.

After a NC reaction, the free neutron captures on a nucleus in the detector and results in the production of one or more gamma-rays (one 6.25 MeV gamma-ray for a capture on a deuteron, and one or more gamma-rays with a total energy of 8.6 MeV for a capture on ³⁵Cl). The gamma-ray(s) usually Compton-scatters an electron which, in turn, emits Čerenkov radiation. The time delay between the NC reaction and the production of Čerenkov photons is typically tens of milliseconds or less.

SNO's photomultiplier tubes detect the Čerenkov photons when a physics event occurs in the detector. The PMT hit times and charge information are recorded for each event. Since the locations of the PMTs are known precisely, the PMT hit times can be used to reconstruct the location and direction of propagation of the Čerenkov light-producing

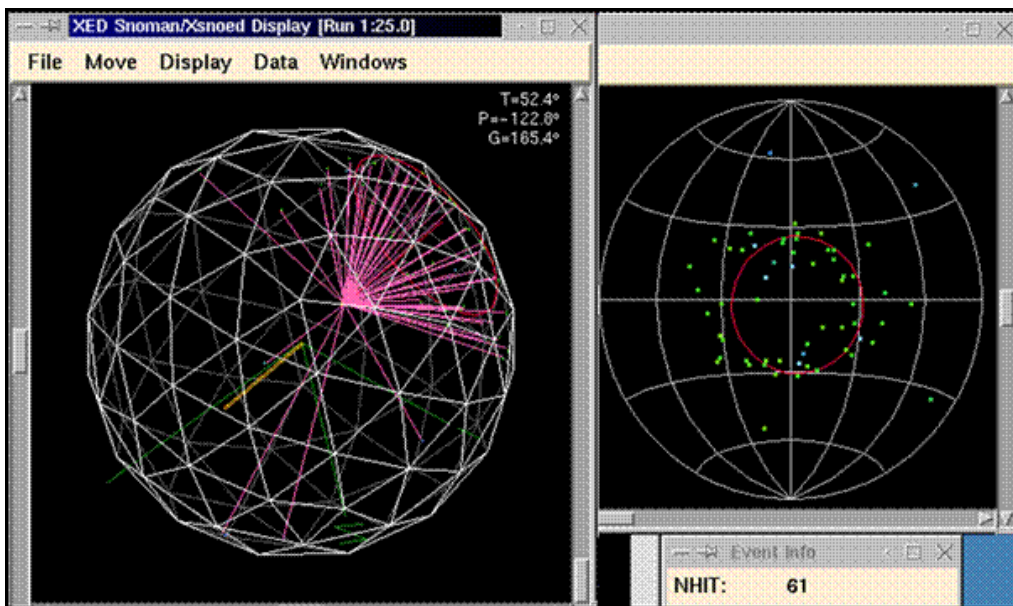


Figure 3: A physics event in SNO's event display. The image on the left shows SNO's PMT support structure and the reconstructed Čerenkov photon trajectories in the event. The image on the right shows the same event projected onto a flat circular surface; the dots indicate hit PMTs. The event vertex and electron direction are reconstructed using the hit PMT locations and times. The electron energy can be estimated by the number of PMT hits.

electrons. The number of emitted Čerenkov photons is proportional to the electron energy, so the number of PMT hits is used to estimate the energy of the electron in a physics event. An example of a reconstructed event as seen in SNO's event display is shown in Figure 3.

5. Solar neutrino results from the D₂O phase

During the first phase of SNO, the acrylic vessel contained pure D₂O only. In total, there are 306.4 live days of data in the first phase. Three solar neutrino papers have been published using all or part of this data set. For the first paper, the CC and ES rates and corresponding neutrino fluxes were measured [10]. The NC and CC rates were measured for the second paper [11], and the asymmetry between the night-time and day-time fluxes was measured for the third paper [12]. For each of these measurements, it was not possible to differentiate CC, ES and NC interactions on an event-by-event basis; instead, a statistical separation was performed. Three different observables were used to discriminate amongst the different reactions: the estimated electron kinetic energy, T , the cosine of the angle between the Sun-Earth vector and the estimated direction of propagation of the electron, $\cos \theta_{\text{sun}}$, and the radius at which the electron was reconstructed, R . Figure 4 shows the distributions of these observables for the CC, ES, and NC reactions during the pure D₂O phase.

5.1. SNO's charged current measurement in D₂O

From the first paper [10], the measured ⁸B neutrino fluxes (assuming no neutrino flavour change) are

$$\phi_{\text{SNO}}^{\text{CC}}(\nu_e) = 1.75 \pm 0.07(\text{stat})_{-0.11}^{+0.12}(\text{syst}) \pm 0.05(\text{theor}) \times 10^6 \text{ cm}^{-2}\text{s}^{-1} \text{ and} \quad (2)$$

$$\phi_{\text{SNO}}^{\text{ES}}(\nu_x) = 2.39 \pm 0.34(\text{stat})_{-0.14}^{+0.16}(\text{syst}) \times 10^6 \text{ cm}^{-2}\text{s}^{-1}, \quad (3)$$

where the first error is statistical, the second is systematic, and $\phi_{\text{SNO}}^{\text{CC}}(\nu_e)$ has a theoretical uncertainty due to uncertainty in the CC cross section. The kinetic energy threshold for this analysis is 6.75 MeV. There is not a significant

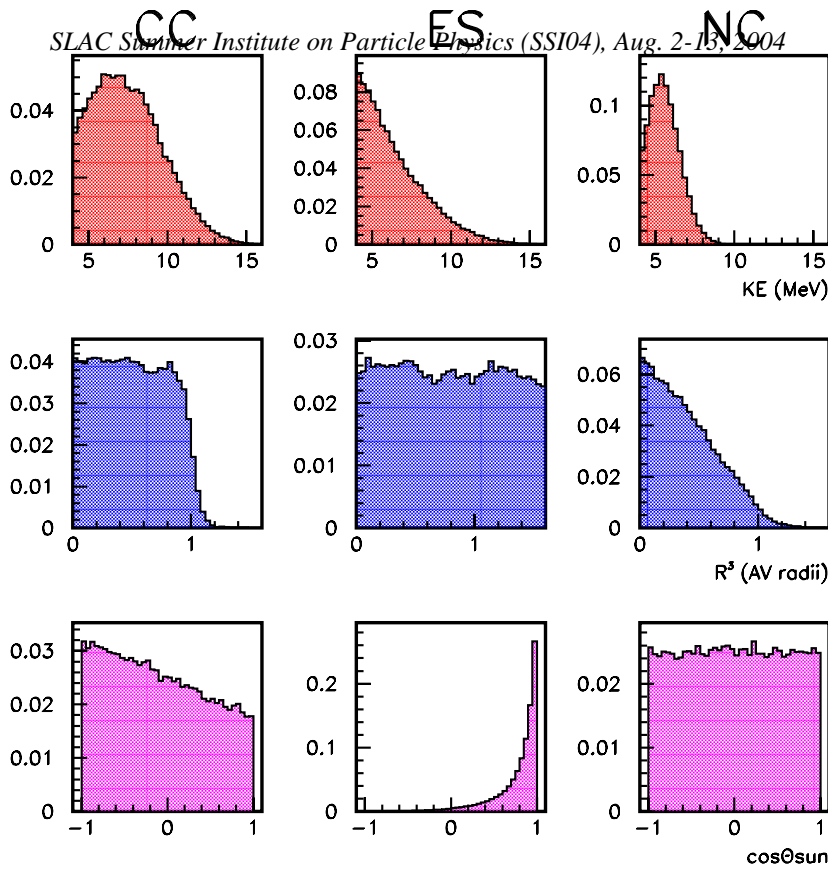


Figure 4: Observables used to separate CC (left column), ES (middle column), and NC (right column) signals. The three variables used for D₂O analyses are the estimated electron kinetic energy, KE, the radius at which the electron was reconstructed, R, and the cosine of the angle between the Sun-Earth vector and the estimated direction of propagation of the electron, $\cos \theta_{\text{sun}}$. For the radius, $(R/600 \text{ cm})^3$ is plotted so that the distribution is weighted by volume. The value $(R/600 \text{ cm})^3 = 1$ corresponds to the location of the acrylic vessel. In order to reduce the level of background in the solar neutrino data set, a fiducial volume cut of $(R/600 \text{ cm})^3 < 0.77$ is applied to the data.

difference between $\phi_{\text{SNO}}^{\text{CC}}(\nu_e)$ and $\phi_{\text{SNO}}^{\text{ES}}(\nu_x)$ as the statistical uncertainty on the latter is quite large. However, if one compares $\phi_{\text{SNO}}^{\text{CC}}(\nu_e)$ to Super-Kamiokande's more precise ES measurement, $\phi_{\text{SK}}^{\text{ES}}(\nu_x) = 2.32 \pm 0.03_{-0.07}^{+0.08} \times 10^6 \text{ cm}^{-2}\text{s}^{-1}$ [2], the discrepancy is at the 3.3 sigma level. This was the first direct evidence that there are active flavour neutrinos, other than ν_e , taking part in the ES reaction.

5.2. SNO's neutral current measurement in D₂O

SNO's second measurement from the D₂O phase determined the flux of all active neutrino flavours via the NC reaction, $\phi_{\text{SNO}}^{\text{NC}}(\nu_x)$ [11]. The CC flux, $\phi_{\text{SNO}}^{\text{CC}}(\nu_e)$, was also measured more precisely than before, since this analysis used a lower kinetic energy threshold ($T_{\text{eff}} \geq 5 \text{ MeV}$) and a larger data set. The results from this measurement are

$$\phi_{\text{SNO}}^{\text{CC}}(\nu_e) = 1.76_{-0.05}^{+0.06}(\text{stat}) \pm 0.09(\text{syst}) \times 10^6 \text{ cm}^{-2}\text{s}^{-1}, \quad (4)$$

$$\phi_{\text{SNO}}^{\text{NC}}(\nu_x) = 5.09_{-0.43}^{+0.44}(\text{stat})_{-0.43}^{+0.46}(\text{syst}) \times 10^6 \text{ cm}^{-2}\text{s}^{-1}. \quad (5)$$

The 5.3 sigma difference between the NC and CC fluxes is clear evidence that there are neutrinos other than ν_e taking part in the NC reaction. In other words, this is evidence of ν_e flavour change to ν_μ and/or ν_τ . In addition to providing evidence for ν_e flavour change, the measured NC flux is consistent with the flux of ⁸B neutrinos predicted by the Standard Solar Model, $\phi_{\text{SSM}} = 5.82 \pm 1.34 \times 10^6 \text{ cm}^{-2}\text{s}^{-1}$ [1]. This demonstrates that the SSM does an excellent job of describing the physical processes that occur in the extreme environment of the Sun's core. Figure 5 summarizes SNO's CC, NC and ES measurements from the D₂O phase.

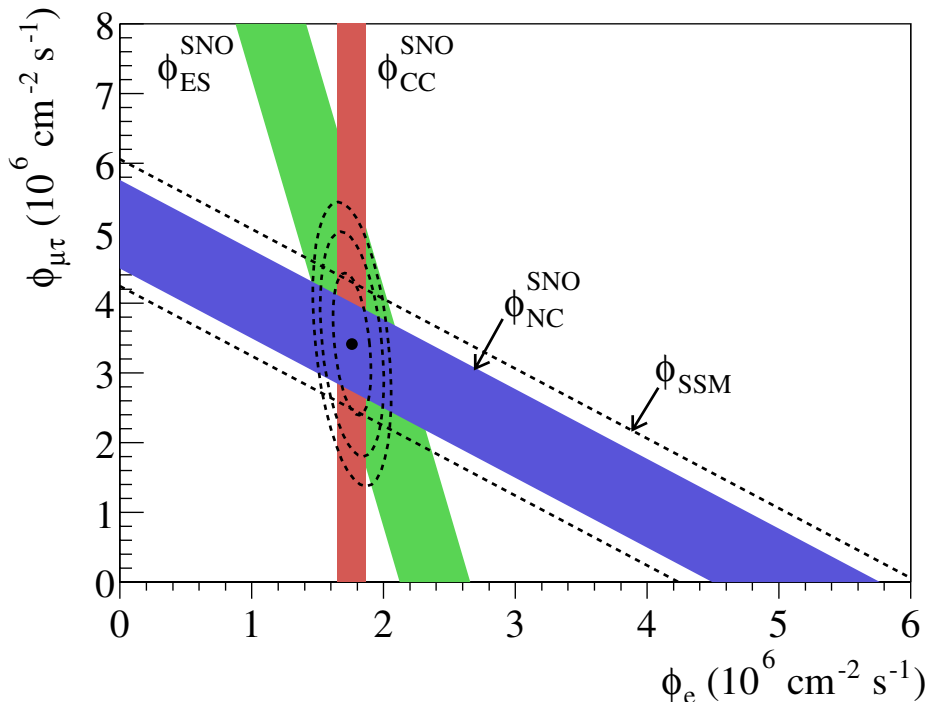


Figure 5: SNO's CC, NC and ES measurements from the D₂O phase. The x- and y-axes are the inferred fluxes of electron neutrinos and muon plus tau neutrinos. Since the NC and ES measurements are sensitive to both ν_e and ν_μ/ν_τ , the ES and NC bands have definite slopes. The CC measurement is sensitive to ν_e only, so has an infinite slope. The widths of the bands represent the uncertainties of the measurements. The intersection of the three bands gives the best estimate of $\phi_{\mu\tau}$ and ϕ_e . The dashed ellipses around the best fit point give the 68%, 95%, and 99% confidence level contours for $\phi_{\mu\tau}$ and ϕ_e . The flux of neutrinos predicted by the SSM is indicated by ϕ_{SSM} .

5.3. SNO's night-day flux asymmetry measurement in D₂O

In addition to measuring the time integrated fluxes, the difference between the solar neutrino fluxes at night and day has also been studied [12]. If the mixing of solar neutrino flavours is due to interactions with matter (the MSW effect) [13, 14], then ν_e might regenerate while passing through the Earth at night time. For more details on the MSW effect, see Boris Kayser's lectures in these proceedings [8]. The probability to regenerate depends on the neutrino mixing parameters, Δm_{12}^2 ($=m_1^2 - m_2^2$, the difference of the squared neutrino masses) and θ_{12} (the solar neutrino mixing angle), the path length of the neutrinos through the Earth, and the local electron density that the neutrinos encounter. SNO has determined the night-day asymmetry $\mathcal{A} = 2(\phi_{\text{night}} - \phi_{\text{day}})/(\phi_{\text{night}} + \phi_{\text{day}})$ for the flux of ν_e under two different assumptions. The first assumption is that \mathcal{A}_{NC} may be non-zero (possible if there is matter enhanced mixing with sterile neutrinos). The asymmetry of the NC rate was allowed to float in a fit to the data that simultaneously determined the asymmetries of the CC and NC rates. The result of the fit was

$$\mathcal{A}_{\text{CC}} = \mathcal{A}_e = (14.0 \pm 6.3^{+1.5}_{-1.4})\%, \quad \mathcal{A}_{\text{NC}} = (-20.4 \pm 16.9^{+2.4}_{-2.5})\%. \quad (6)$$

The second assumption is that there is no mixing with sterile neutrinos. When \mathcal{A}_{NC} is fixed at zero, SNO measures

$$\mathcal{A}_e = (7.0 \pm 4.9^{+1.3}_{-1.2})\%, \quad \mathcal{A}_{\text{NC}} = 0. \quad (7)$$

Both of these results are consistent with no night-day asymmetry.

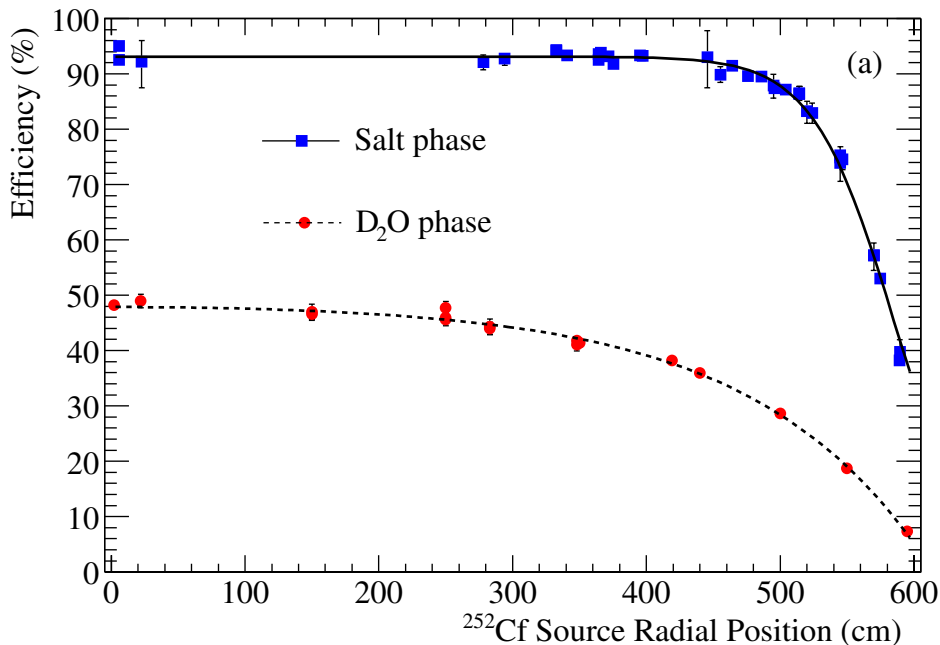


Figure 6: SNO's neutron capture efficiencies for the pure D_2O and salt phases. The neutron capture efficiency is measured with neutrons from a radioactive ^{252}Cf source. The source was deployed at a number of different positions in the detector, in order to obtain a thorough understanding of the neutron capture efficiency.

6. Solar neutrino results from the salt phase

6.1. Motivation for adding salt to the heavy water

At the start of SNO's second data taking phase, 1950 kg of pure NaCl were added to the D_2O . The salt was added to improve SNO's sensitivity to the neutral current reaction. SNO's sensitivity is improved for three reasons:

- the neutron capture efficiency is increased;
- the neutron detection efficiency is increased;
- the NC signal is more easily distinguished from the CC signal.

The neutron capture efficiency is increased because ^{35}Cl has a 44 mb neutron capture cross-section, whereas the neutron capture cross-section on ^2H is 0.0005 mb. Figure 6 shows the measured neutron capture efficiencies from the D_2O and salt phases of SNO for a radioactive ^{252}Cf source. The detection efficiency is increased because the energy of the gamma-rays produced in n-capture on ^{35}Cl is 8.6 MeV, while the energy of the gamma-ray produced in n-capture on ^2H is 6.25 MeV. This means that a larger fraction of n-captures on ^{35}Cl produce enough light to be above the analysis's electron kinetic energy threshold of 5.5 MeV. The improved neutron capture and gamma-ray detection efficiencies increase the neutron detection efficiency from 14.4% in pure D_2O to 39.9% in D_2O plus salt.

The third advantage of adding salt to the D_2O is that it allows the NC signal to be more easily distinguished from the CC signal. This improvement in signal separation is achieved because of the multiple gamma-rays that are produced by n-capture on ^{35}Cl ; on average, 2.5 gammas are produced per capture. Each gamma can Compton-scatter an electron, thereby producing Čerenkov light. Since the distribution of gammas is isotropic, the Čerenkov light distribution from NC events in the salt phase will have PMT hit patterns that are more isotropic than CC or ES events, which produce a single Čerenkov electron. To take advantage of this difference, a variable that measures the

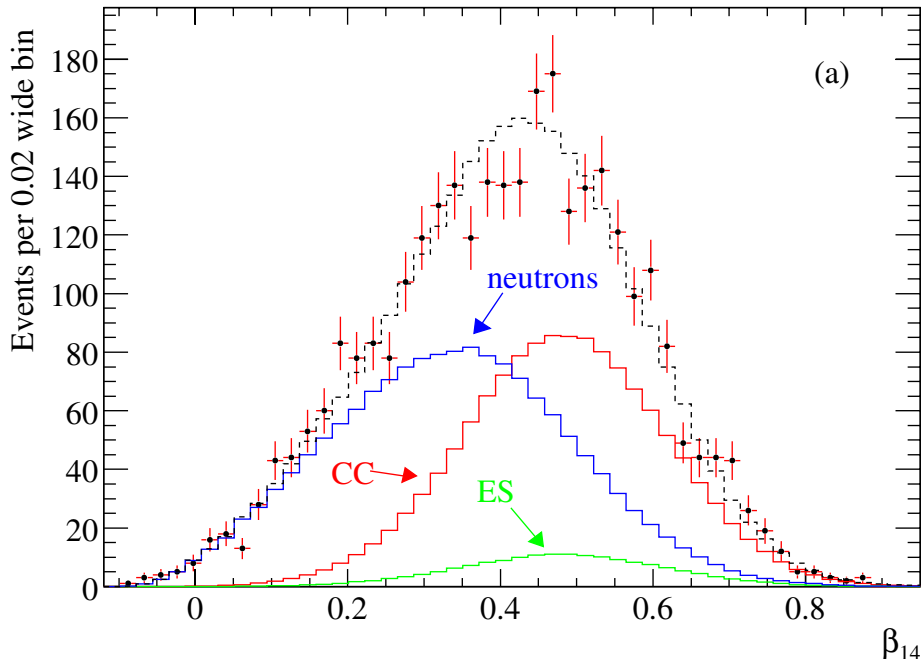


Figure 7: Event isotropy variable, β_{14} , distribution for neutrons (from NC reactions and background), and CC and ES reactions. Large values of β_{14} indicate less isotropic light distribution in an event. The data points show the neutrino data from the salt phase. The dashed histogram is the sum of the Monte Carlo probability density functions scaled by the fitted numbers of events.

isotropy of the PMT hit pattern in an event is constructed. The event isotropy variable, β_{14} , is a sum of Legendre polynomials that optimizes the discrimination between the NC and CC/ES signals:

$$\beta_{14} = \beta_1 + 4\beta_4, \quad (8)$$

where

$$\beta_1 = \frac{2}{N(N-1)} \sum_{i=1}^{N-1} \sum_{j=i+1}^N \cos \theta_{ij}, \quad (9)$$

$$\beta_4 = \frac{2}{N(N-1)} \sum_{i=1}^{N-1} \sum_{j=i+1}^N \frac{1}{64} (9 + 20 \cos 2\theta_{ij} + 35 \cos 4\theta_{ij}). \quad (10)$$

Here, N is the number of PMT hits, and θ_{ij} is the angle between two hit PMTs. This variable is similar to event shape variables that are used in collider physics (e.g. event thrust, sphericity, etc.). Figure 7 shows the distribution of the event isotropy variable for the different solar neutrino reactions.

6.2. Calibration of SNO during the salt phase

Since the neutrino fluxes are measured by fitting Monte Carlo (MC) distributions to the data, it is necessary to verify that the detector response is accurately modelled. This is achieved by taking data with a number of calibration sources and comparing the data to the simulated data for the same sources. The most important calibration sources are a diffuse laser light source, a ^{16}N triggered gamma-ray source [15], and a ^{252}Cf neutron source. The laser source is used to measure the optical properties of the detector. The measured optical properties are then used in the

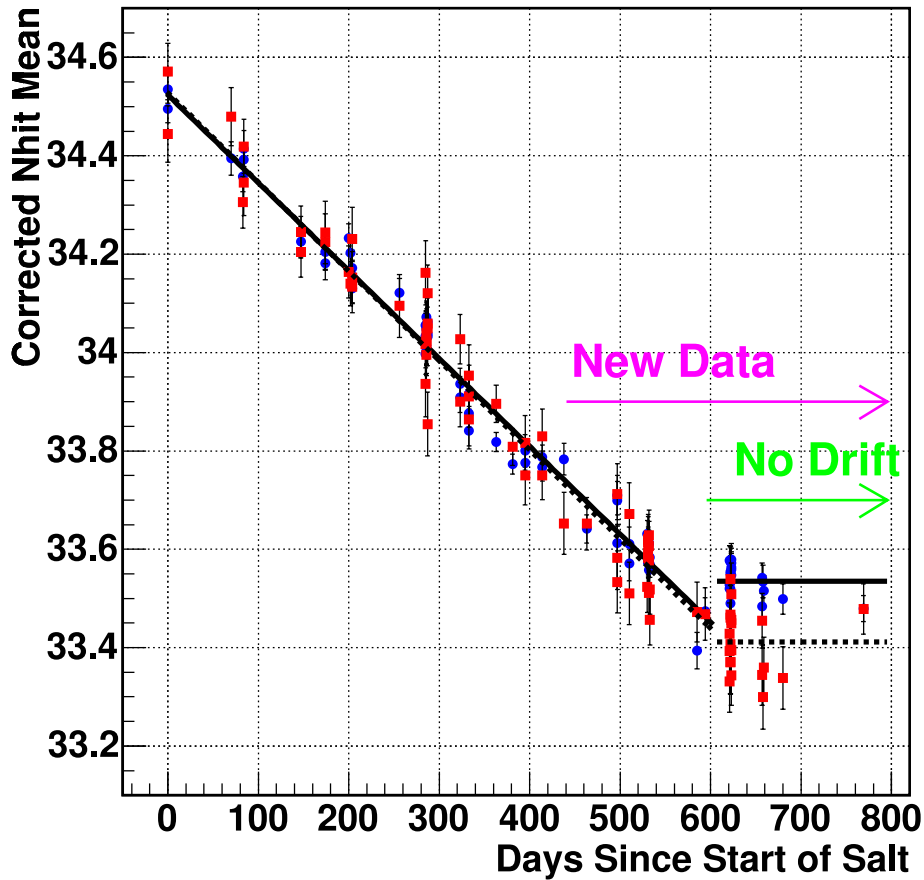


Figure 8: Comparison of ^{16}N gamma-ray source data and MC. The data points are shown by the red/grey squares, and the MC are shown by the blue/black circles. The mean number of hit PMTs per ^{16}N decay, N_{hit} , is plotted as a function of time during the salt phase of data taking. The number of hit PMTs provides an estimate of the energy of an event. The energy response changes slowly with time and is well modelled by the simulation. The data used for the analysis presented here do not include the “New Data” indicated on the plot.

simulation of the other calibration sources and the physics signals and backgrounds. The ^{16}N gamma-ray source is used to calibrate the energy response of the detector, and to verify the modelling of the event isotropy variable. As mentioned in Section 6.1, the ^{252}Cf neutron source is used to calibrate the neutron detection efficiency. Differences between the calibration MC and data are considered sources of systematic uncertainty. Figure 8 shows the good agreement between the MC and the real data for the ^{16}N source data.

6.3. SNO data set and data reduction

The salt data for SNO’s most recent publication were collected between July 2001 and October 2002. There were a total of 254.2 live days during this time. The raw data set consists of 435,721,068 triggers. Several stages of data reduction were necessary to select a relatively background-free neutrino data set. The first stage of reduction involved the removal of instrumental backgrounds. After that, cosmic ray muon events and their spallation products were removed by vetoing events with hits in the outward-looking PMTs (cosmic ray muons) and cutting any events that

Source	Events
Deuteron photodisintegration	$73.1^{+24.0}_{-23.5}$
${}^2\text{H}(\alpha, \alpha)pn$	2.8 ± 0.7
${}^{17,18}\text{O}(\alpha, n)$	1.4 ± 0.9
Fission, atmospheric ν (NC + sub-Cherenkov threshold CC)	23.0 ± 7.2
Terrestrial and reactor $\bar{\nu}$'s	2.3 ± 0.8
Neutrons from rock	≤ 1
${}^{24}\text{Na}$ activation	8.4 ± 2.3
n from CNO ν 's	0.3 ± 0.3
Total internal neutron background	$111.3^{+25.3}_{-24.9}$
Internal γ (fission, atmospheric ν)	5.2 ± 1.3
${}^{16}\text{N}$ decays	< 2.5 (68% CL)
External-source neutrons (from fit)	$84.5^{+34.5}_{-33.6}$
Cherenkov events from $\beta - \gamma$ decays	< 14.7 (68% CL)
“AV events”	< 5.4 (68% CL)

Table I: Background events in neutrino data set in salt phase (254.2 live days). The “external-source neutrons” originate at the acrylic vessel. The size of this background is determined from the fit to the data (see Section 6.6 for more details). “AV events” are high energy, isotropic events from an unknown source, located on the acrylic vessel.

occurred less than 20 s after the muon (spallation products). At this stage of data reduction, candidate neutrino events were reconstructed; those events with PMT time distributions or fit locations incompatible with neutrino events were removed from the data set. Finally, a fiducial volume cut of $R < 550$ cm and an electron kinetic energy threshold cut of 5.5 MeV were imposed to remove all but a small number of background events. This left 3055 candidate neutrino events. Approximately 200 of these events ($\sim 7\%$) are estimated to be background events.

6.4. Backgrounds in the salt data set

As mentioned in Section 3, the reduction of natural radioactivity is vital to the success of SNO. Two of the many backgrounds that are closely monitored are U and Th. The concentrations of U and Th in the D_2O are measured on a regular basis by removing samples of D_2O and measuring the levels of radioactive daughters of U and Th [16, 17]. Figure 9 shows the measured U and Th levels as a function of time. The levels of both U and Th are lower than the design goals. These assay results can be compared to “*in situ*” measurements of the levels of U and Th: *in situ* measurements determine the levels of bismuth and thallium in the D_2O by studying data below the 5.5 MeV kinetic energy threshold. The measured levels of bismuth and thallium are used to calculate the concentrations of U and Th in the D_2O . The results of the assays and the *in situ* measurements are in agreement, and since the *in situ* measurements are more precise, they are used to estimate the U and Th backgrounds.

A summary of all the sources of background in this data set is provided in Table I. The largest sources of background are neutrons from the photodisintegration of deuterons (requires $E_\gamma > 2.2$ MeV), and neutrons from the acrylic vessel, “external-source neutrons”.

6.5. Systematic uncertainties in salt phase measurements

A number of sources of systematic uncertainty have been investigated for this analysis. Table II lists all the significant sources of uncertainty. The dominant sources of systematic uncertainty on the NC flux measurement are the energy scale, the radial accuracy, and the mean of the simulated isotropy distribution. The uncertainty in the energy scale is determined from the comparison of ${}^{16}\text{N}$ calibration source data to MC. The uncertainty in the reconstructed location of the radius of the event vertex (radial accuracy) translates into an uncertainty in the fiducial

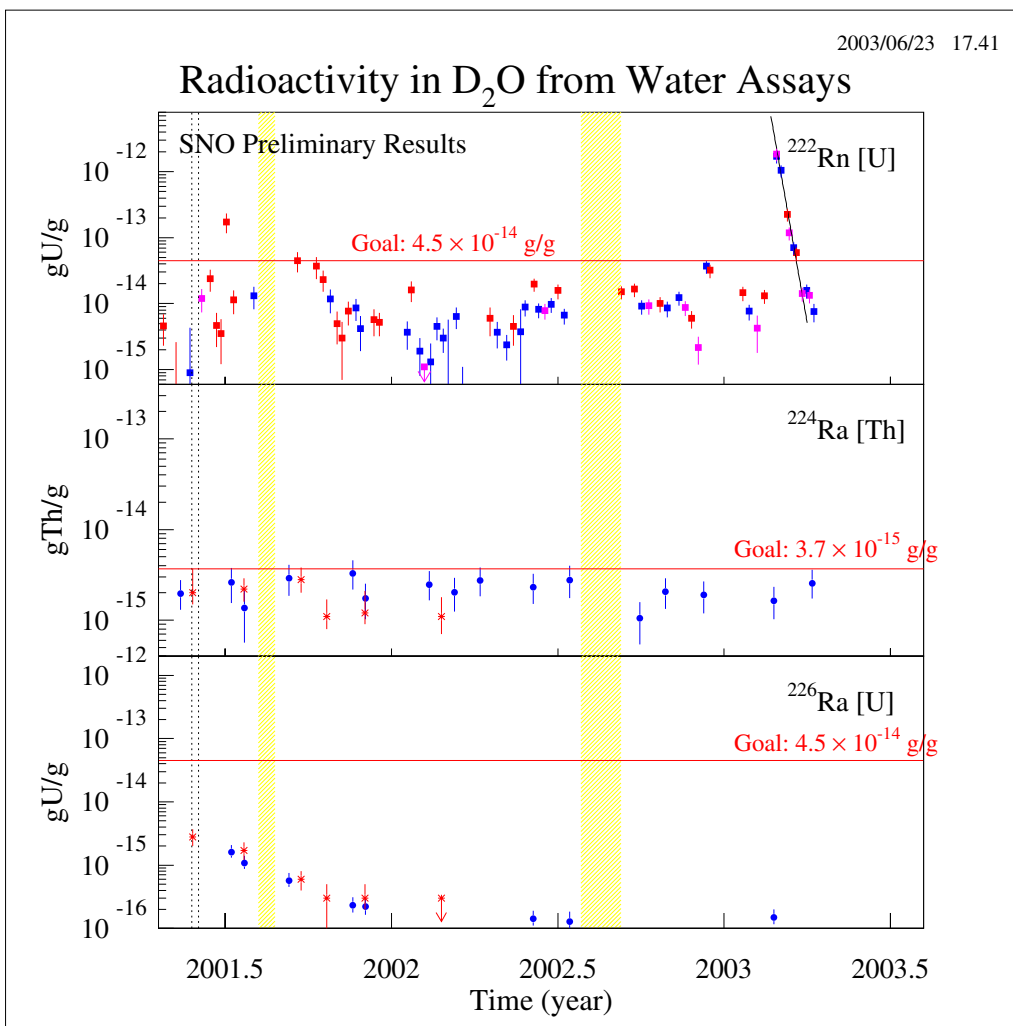


Figure 9: Measured U and Th content in SNO's D₂O. The concentrations of U and Th (in grams of U or Th per gram of D₂O) are plotted as a function of time. The radioactive isotopes ²²²Rn and ²²⁶Ra are measured to estimate the amount of U in the heavy water. The amount of Th in the heavy water is estimated by measuring ²²⁴Ra. SNO's U and Th contamination goals are indicated on the plots by horizontal lines. The goals correspond to the equivalent of one background neutron per day.

volume. The fiducial volume is used to calculate the neutrino fluxes from the measured event rate. The uncertainty in the simulated isotropy distributions is determined from a comparison of calibration data to MC. The dominant sources of systematic uncertainty on the CC flux are the radial accuracy and the mean of the simulated isotropy distribution, while the dominant sources of uncertainty on the ES flux are the radial accuracy and the angular resolution. The angular resolution is particularly important for determining the ES flux, as the $\cos\theta_{\text{sun}}$ distribution is the most powerful variable for discriminating ES reactions from the other reactions. The $\cos\theta_{\text{sun}}$ distribution is strongly forward-peaked for ES events, while it is fairly flat for CC and NC events (see Figure 10).

6.6. Measurement of CC, NC, and ES fluxes

The CC, NC, and ES event rates are measured by comparing the probability density functions (PDFs), determined from simulated data for all signals and backgrounds, to the neutrino data. An unbinned extended maximum likelihood

Source	NC uncert. (%)	CC uncert. (%)	ES uncert. (%)
Energy scale	-3.7,+3.6	-1.0,+1.1	± 1.8
Energy resolution	± 1.2	± 0.1	± 0.3
Energy non-linearity	± 0.0	-0.0,+0.1	± 0.0
Radial accuracy	-3.0,+3.5	-2.6,+2.5	-2.6,+2.9
Vertex resolution	± 0.2	± 0.0	± 0.2
Angular resolution	± 0.2	± 0.2	± 2.4
Isotropy mean †	-3.4,+3.1	-3.4,+2.6	-0.9,+1.1
Isotropy resolution	± 0.6	± 0.4	± 0.2
Radial energy bias	-2.4,+1.9	± 0.7	-1.3,+1.2
Vertex Z accuracy †	-0.2,+0.3	± 0.1	± 0.1
Internal background neutrons	-1.9,+1.8	± 0.0	± 0.0
Internal background γ 's	± 0.1	± 0.1	± 0.0
Neutron capture	-2.5,+2.7	± 0.0	± 0.0
Cherenkov backgrounds	-1.1,+0.0	-1.1,+0.0	± 0.0
“AV events”	-0.4,+0.0	-0.4,+0.0	± 0.0
Total experimental uncertainty	-7.3,+7.2	-4.6,+3.8	-4.3,+4.5
CC, NC and ES cross sections	± 1.1	± 1.2	± 0.5

Table II: Systematic uncertainties on the CC, NC, and ES fluxes for the energy-unconstrained analysis of the salt data set. The † symbol denotes a systematic uncertainty that is anti-correlated between the CC and NC fluxes.

fit is performed. The numbers of neutron¹, CC, ES, and “external neutron” events are free parameters in the analysis. Two separate fits are performed. For the first fit, three variables are used to calculate the joint likelihood variable that is compared in the MC and the data: event isotropy, $\cos\theta_{\text{sun}}$, and the radial position of the event vertex. This fit is unconstrained in energy, so it provides a model-independent measurement of the fluxes of the different neutrino flavours. If the MSW effect contributes to neutrino flavour change, then the CC and ES kinetic energy distributions may be distorted. By not including energy in this fit, no assumption is made about the shape of the CC and ES energy spectra. All of SNO’s results from the pure D₂O phase assume that the CC and ES energy spectra are undistorted.

The second fit uses the estimated electron kinetic energy as a fourth variable in the likelihood calculation. The energy spectra for the ES and CC reactions are constrained to follow the expected spectra, assuming that neutrino flavour mixing is not energy dependent. The results of this fit have better precision, but are not model-independent.

The PDFs of the four variables used for this analysis are shown in Figures 7, 10, 11 and 12. For all of the variables, there is acceptable agreement between the summed MC PDFs (dashed histograms) and the data.

The results of the energy-unconstrained (three variable) fit, in units of $10^6 \text{ cm}^{-2}\text{s}^{-1}$, are

$$\begin{aligned}\phi_{\text{CC}}^{\text{SNO}} &= 1.59_{-0.07}^{+0.08}(\text{stat})_{-0.08}^{+0.06}(\text{syst}), \\ \phi_{\text{ES}}^{\text{SNO}} &= 2.21_{-0.26}^{+0.31}(\text{stat}) \pm 0.10(\text{syst}), \\ \phi_{\text{NC}}^{\text{SNO}} &= 5.21 \pm 0.27(\text{stat}) \pm 0.38(\text{syst}).\end{aligned}$$

In the same units, the results of the energy-constrained (four variable) fit are

$$\phi_{\text{CC}}^{\text{SNO}} = 1.70 \pm 0.07(\text{stat})_{-0.10}^{+0.09}(\text{syst}),$$

¹This includes neutron events from NC reactions and background sources. To calculate the NC rate, the estimated neutron background is subtracted from the measured number of neutrons.

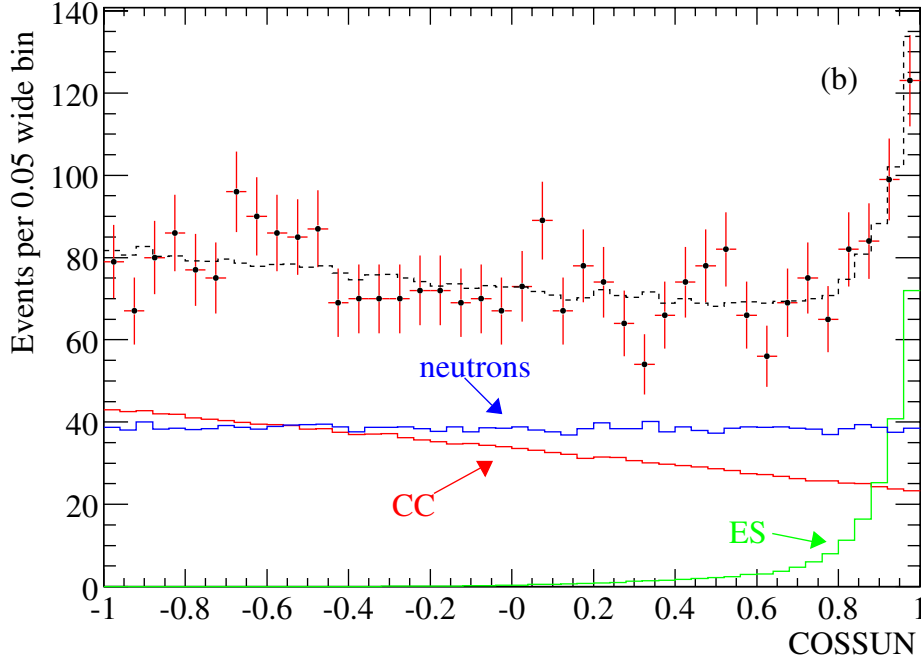


Figure 10: Distributions of $\cos \theta_{\text{sun}}$ for neutrons, CC events, and ES events, summed MC PDFs (dashed histogram), and real neutrino data (data points). Large values of $\cos \theta_{\text{sun}}$ indicate that the electron's direction of propagation points in the same direction as the Sun to Earth direction.

$$\begin{aligned}\phi_{\text{ES}}^{\text{SNO}} &= 2.13_{-0.28}^{+0.29}(\text{stat})_{-0.08}^{+0.15}(\text{syst}), \\ \phi_{\text{NC}}^{\text{SNO}} &= 4.90 \pm 0.24(\text{stat})_{-0.27}^{+0.29}(\text{syst}).\end{aligned}$$

In both cases, $\phi_{\text{CC}}^{\text{SNO}}$ and $\phi_{\text{NC}}^{\text{SNO}}$ are not consistent with each other. The ratio of the energy-unconstrained ${}^8\text{B}$ flux measured with the CC and NC reactions is $\phi_{\text{CC}}^{\text{SNO}}/\phi_{\text{NC}}^{\text{SNO}} = 0.306 \pm 0.026(\text{stat}) \pm 0.024(\text{syst})$. Consequently, these measurements provide further evidence of solar neutrino flavour change. These results are consistent with SNO's previous results from the pure D_2O phase. Again, the measured $\phi_{\text{NC}}^{\text{SNO}}$ is consistent with the flux of ${}^8\text{B}$ neutrinos predicted by the Standard Solar Model, $\phi_{\text{SSM}} = 5.82 \pm 1.34 \times 10^6 \text{ cm}^{-2}\text{s}^{-1}$ [1].

6.7. Implications for neutrino mixing parameters

By making precise measurements of the flux of solar neutrinos, SNO is able to constrain the allowed parameter space for the neutrino mixing parameters Δm_{12}^2 and θ_{12} . If vacuum oscillation is the mechanism for neutrino flavour change, the survival probability for ν_e produced in the Sun to be detected as ν_e at the Earth is given by

$$P_{\nu_e \rightarrow \nu_e} = 1 - \sin^2 2\theta_{12} \sin^2 \left(\frac{1.27 \Delta m_{12}^2 L}{E} \right), \quad (11)$$

where L is the separation between the neutrino source and the detector in km, E is the neutrino energy in GeV, and Δm_{12}^2 is the difference of the squared neutrino masses in eV^2 . The parameters Δm_{12}^2 and θ_{12} must be replaced by modified terms that include Δm_{12}^2 and θ_{12} if matter enhanced oscillations contribute to neutrino flavour change (see Boris Kayser's talk for more details [8]). The survival probability is equivalent to the ratio of the neutrino fluxes measured with the CC and NC reactions, $\phi_{\text{CC}}^{\text{SNO}}/\phi_{\text{NC}}^{\text{SNO}}$. So, by measuring $\phi_{\text{CC}}^{\text{SNO}}/\phi_{\text{NC}}^{\text{SNO}}$, SNO is able to constrain the allowed values of Δm_{12}^2 and θ_{12} .

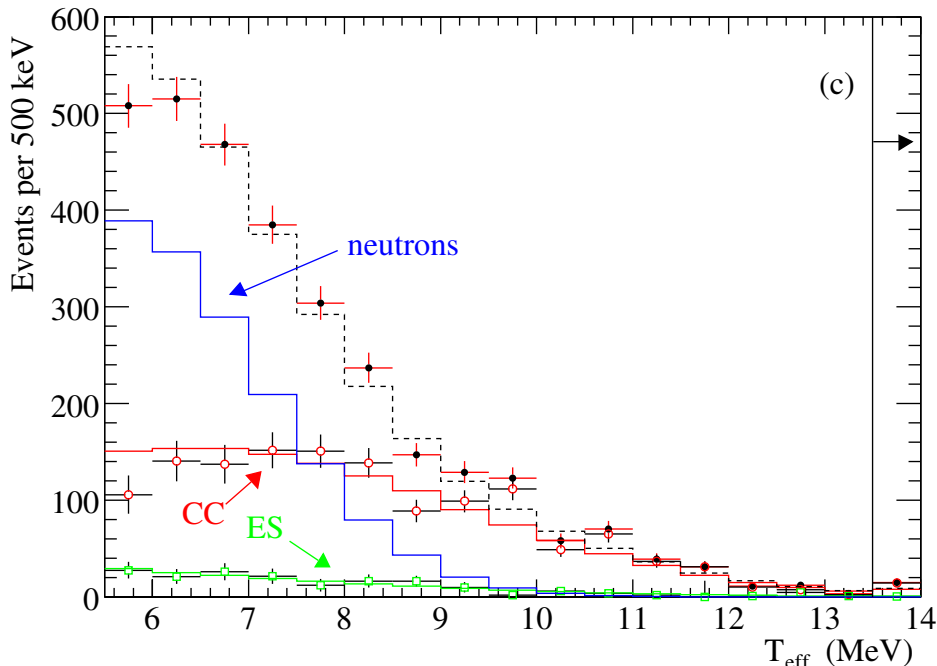


Figure 11: Distributions of electron kinetic energy, T_{eff} , for neutrons, CC events, and ES events, summed MC PDFs (dashed histogram), and real neutrino data (data points). Events with $14 \text{ MeV} < T_{\text{eff}} < 20 \text{ MeV}$ are combined in the same bin.

For each point in the two dimensional neutrino mixing parameter space, the predicted CC, NC and ES fluxes are calculated. These predicted fluxes are compared to the measured fluxes, and the χ^2 difference between the measured values and the predicted values is determined for each point in the mixing parameter space. This results in a map of χ^2 values that can be expressed in terms of confidence intervals for the mixing parameters, by calculating $\Delta\chi^2$ with respect to the minimum χ^2 .

Figure 13 shows the allowed mixing parameter space using only SNO data to constrain the mixing parameters. A number of different isolated regions yield acceptable agreement with the data. The allowed parameter space can be constrained further by performing a global fit to all solar neutrino data and data from the Kamland reactor neutrino experiment [18]. Figure 14 shows that the best fit point from the global analysis is $\Delta m_{12}^2 = 7.1_{-0.3}^{+1.0} \times 10^{-5} \text{ eV}^2$ and $\theta_{12} = 32.5_{-1.6}^{+1.7}$ degrees. This result suggests that the MSW effect in the Sun is the mechanism for ${}^8\text{B}$ solar neutrino flavour change. This region in the mixing parameter space is referred to as the Large Mixing Angle (LMA) solution. This value of θ_{12} disfavors the maximal mixing solution ($\theta_{12} = 45$ degrees) at a level equivalent to 5.4σ . The maximal mixing solution had previously been favoured by some theorists.

7. Recent non-solar neutrino results

7.1. Invisible nucleon decay

In addition to SNO's solar neutrino measurements, two non-solar neutrino analyses have recently been completed. The first of these is a search for "invisible" nucleon decay [19]. An example of an invisible nucleon decay is $N \rightarrow \nu\nu\nu$. The three neutrinos would not be detected, but if the decay occurred in ${}^{16}\text{O}$, the de-excitation of the nucleus would produce gamma-rays with approximately 6 to 7 MeV. In SNO, gamma-rays of this energy look very similar to the NC signal from neutron capture. Consequently, if the measured NC signal in the pure D_2O phase is compared to the measured NC signal in the salt phase, a limit can be set on the lifetime of neutrons and protons, because the

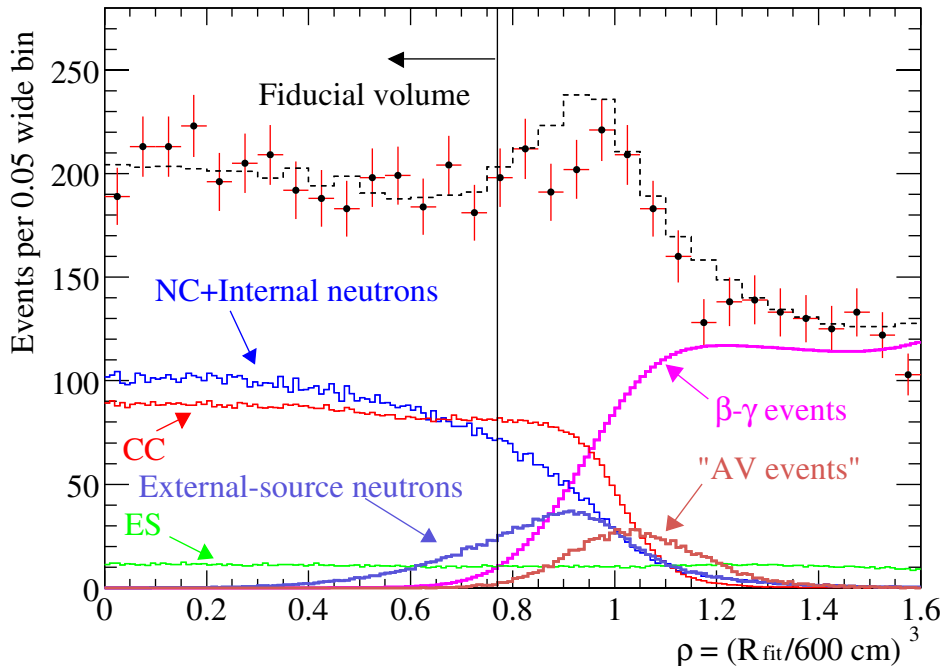


Figure 12: Distributions of volume-weighted radius, ρ , for neutrons, CC events, and ES events, summed MC PDFs (dashed histogram) and real neutrino data (data points). The $\beta - \gamma$ and “AV” events are sources of background whose magnitudes are determined separately from this fit. The acrylic sphere is at $\rho = 1$.

neutron capture efficiency is different in the two phases. A difference between the NC rates in the two phases could be an indication of invisible nucleon decay. In this analysis, the lower limits on the proton and neutron lifetimes for invisible decays are determined:

$$\tau_{inv}^p > 2.1 \times 10^{29} \text{ years, 90\% C.L., and} \quad (12)$$

$$\tau_{inv}^n > 1.9 \times 10^{29} \text{ years, 90\% C.L..} \quad (13)$$

These limits are currently the most stringent limits for invisible nucleon decay.

7.2. Electron anti-neutrino search

It has been hypothesized that solar ν_e might convert to $\bar{\nu}_e$ via Spin Flavour Precession [20–22], or ν_e might decay to final states that include $\bar{\nu}_e$ [23–27]. In either case, if the probability for solar ν_e to produce $\bar{\nu}_e$ is large, then SNO should be able to detect a $\bar{\nu}_e$ signal. SNO is sensitive to $\bar{\nu}_e$ via the reaction



Each of the three final state particles can produce a trigger in SNO. This can lead to double or triple coincidences. The pure D_2O data set has been analyzed to search for double and triple coincidences that are consistent with the $\bar{\nu}_e$ signal. One double coincidence and one triple coincidence have been observed [28]. The expected number of coincidences from background events is $1.68_{-0.45}^{+0.93}$. From these numbers, an upper limit is calculated for the probability for 8B solar ν_e to convert to $\bar{\nu}_e$:

$$\text{Prob}(\nu_e \rightarrow \bar{\nu}_e) < 0.81\%, 90\% \text{ C.L..} \quad (15)$$

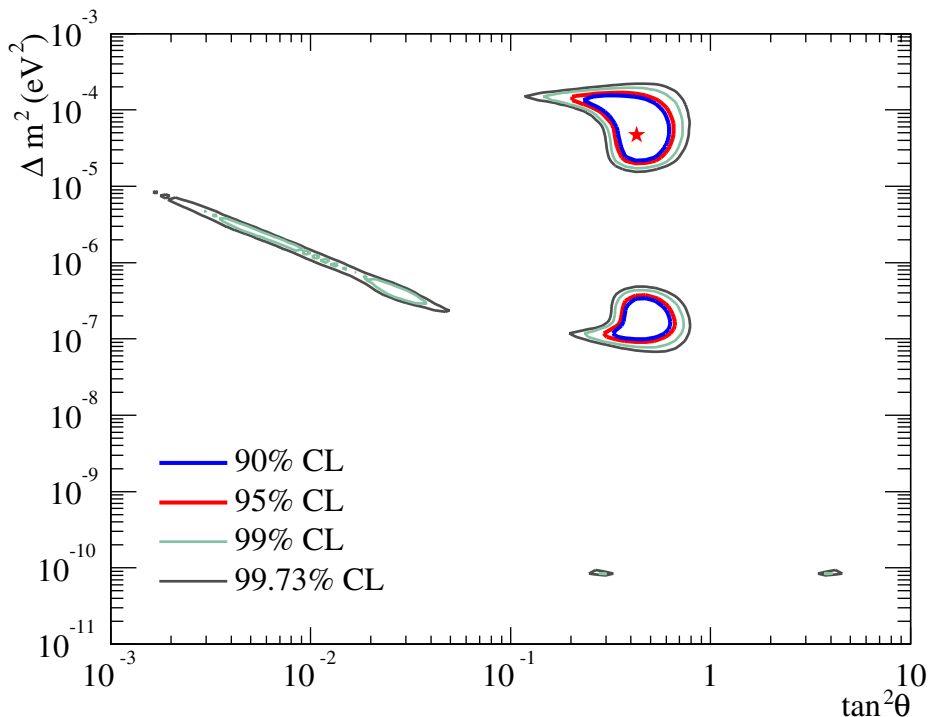


Figure 13: Allowed solar neutrino mixing parameter space using only SNO data. Several distinct allowed regions exist. The best fit point is indicated by the star.

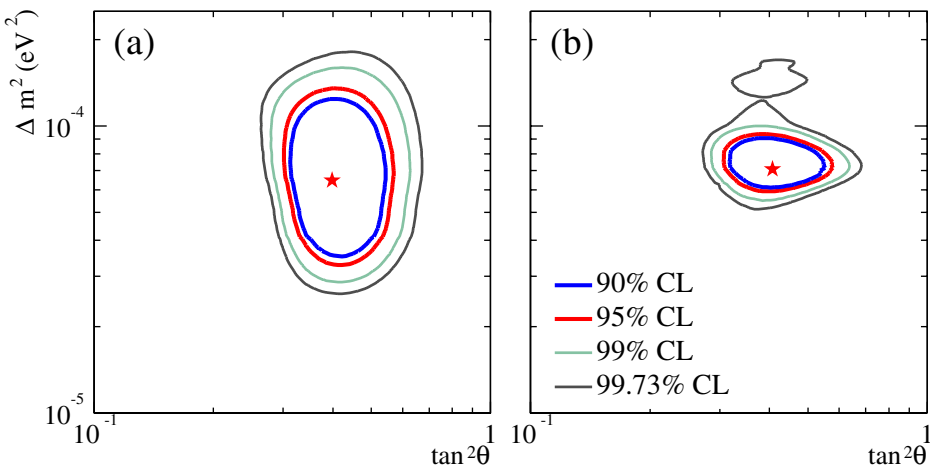


Figure 14: Allowed solar neutrino mixing parameter space using (a) all solar neutrino data and (b) all solar neutrino data plus data from Kamland. The allowed region corresponds to the Large Mixing Angle solution.

8. SNO's future

The final phase of SNO has begun. Proportional counters containing a $^3\text{He-CF}_4$ gas mixture have been deployed in SNO's heavy water and are currently being commissioned. Neutrons produced in NC reactions in the D_2O can capture on ^3He to produce ^3H plus a proton. Both the triton and the proton ionize the gas mixture in the proportional counters, producing a signal in the counters.

Forty proportional counters have been deployed in SNO. Their total length is 398 m. As the counters are only 5 cm in diameter, there are a small number of ^3He nuclei compared to the number of deuterons in the D_2O . However, the

capture cross-section for neutrons on ^3He is 10^7 times larger than the cross-section on ^2H , so most of the neutrons produced in the D_2O will capture in the proportional counters.

As the counters are sensitive to neutron reactions only, they will provide an independent measurement of the flux of all active flavours of solar neutrinos. Also, the counters detect NC events on an event-by-event basis so the anti-correlation that exists between SNO's previous measurements of CC and NC fluxes will not be present. This means that $\phi_{\text{CC}}/\phi_{\text{NC}}$ can be measured more precisely. This should lead to improved precision in the measurement of the solar neutrino mixing angle θ_{12} .

9. Conclusion

SNO has completed its first two phases of data taking: pure D_2O and D_2O plus NaCl . Results from these phases show that approximately $2/3$ of ^8B solar electron neutrinos change flavour to muon or tau neutrinos. The total flux of active-flavour neutrinos is consistent with the flux predicted by the Standard Solar Model. These results represent the solution to the Solar Neutrino Problem that had existed for over thirty years: we now know that solar neutrinos change flavour and the SSM is correct. In addition to SNO's solar neutrino results, searches for invisible nucleon decay and electron anti-neutrinos have recently been completed. SNO is now beginning its third and final phase of data taking with ^3He proportional counters in the D_2O . Data from this last phase should improve the precision of solar neutrino measurements. It might also lead to some unexpected, exciting results.

Acknowledgments

This research was supported by: Canada: NSERC, Industry Canada, NRC, Northern Ontario Heritage Fund, Inco, AECL, Ontario Power Generation, HPCVL, CFI; US: Dept. of Energy; UK: PPARC. We thank the SNO technical staff for their strong contributions.

References

- [1] J. N. Bahcall and M. H. Pinsonneault, *Phys. Rev. Lett.* **92**, 121301 (2004), astro-ph/0402114.
- [2] Super-Kamiokande Collaboration, S. Fukuda *et al.*, *Phys. Rev. Lett.* **86**, 5651 (2001), hep-ex/0103032.
- [3] B. T. Cleveland *et al.*, *Astrophys. J.* **496**, 505 (1998).
- [4] GALLEX Collaboration, W. Hampel *et al.*, *Phys. Lett.* **B447**, 127 (1999).
- [5] GNO Collaboration, M. Altmann *et al.*, *Phys. Lett.* **B490**, 16 (2000), hep-ex/0006034.
- [6] SAGE Collaboration, J. N. Abdurashitov *et al.*, *Phys. Rev.* **C60**, 055801 (1999), astro-ph/9907113.
- [7] G. Gratta, **ECONF in these proceedings** (2004).
- [8] B. Kayser, **ECONF in these proceedings** (2004).
- [9] SNO Collaboration, J. Boger *et al.*, *Nucl. Instrum. Meth.* **A449**, 172 (2000), nucl-ex/9910016.
- [10] SNO Collaboration, Q. R. Ahmad *et al.*, *Phys. Rev. Lett.* **87**, 071301 (2001), nucl-ex/0106015.
- [11] SNO Collaboration, Q. R. Ahmad *et al.*, *Phys. Rev. Lett.* **89**, 011301 (2002), nucl-ex/0204008.
- [12] SNO Collaboration, Q. R. Ahmad *et al.*, *Phys. Rev. Lett.* **89**, 011302 (2002), nucl-ex/0204009.
- [13] S. P. Mikheev and A. Y. Smirnov, *Sov. J. Nucl. Phys.* **42**, 913 (1985).
- [14] L. Wolfenstein, *Phys. Rev.* **D17**, 2369 (1978).
- [15] M. R. Dragowsky *et al.*, *Nucl. Instrum. Meth.* **A481**, 284 (2002), nucl-ex/0109011.
- [16] SNO Collaboration, T. C. Andersen *et al.*, *Nucl. Instrum. Meth.* **A501**, 399 (2003), nucl-ex/0208010.
- [17] SNO Collaboration, T. C. Andersen *et al.*, *Nucl. Instrum. Meth.* **A501**, 386 (2003), nucl-ex/0208015.
- [18] KamLAND Collaboration, K. Eguchi *et al.*, *Phys. Rev. Lett.* **90**, 021802 (2003), hep-ex/0212021.
- [19] SNO Collaboration, S. N. Ahmed *et al.*, *Phys. Rev. Lett.* **92**, 102004 (2004), hep-ex/0310030.

- [20] O. G. Miranda, C. Pena-Garay, T. I. Rashba, V. B. Semikoz, and J. W. F. Valle, Nucl. Phys. **B595**, 360 (2001), hep-ph/0005259.
- [21] B. C. Chauhan and J. Pulido, Phys. Rev. **D66**, 053006 (2002), hep-ph/0206193.
- [22] E. K. Akhmedov and J. Pulido, Phys. Lett. **B553**, 7 (2003), hep-ph/0209192.
- [23] Z. G. Berezhiani, G. Fiorentini, A. Rossi, and M. Moretti, JETP Lett. **55**, 151 (1992).
- [24] A. Acker, A. Joshipura, and S. Pakvasa, Phys. Lett. **B285**, 371 (1992).
- [25] A. Bandyopadhyay, S. Choubey, and S. Goswami, Phys. Rev. **D63**, 113019 (2001), hep-ph/0101273.
- [26] A. S. Joshipura, E. Masso, and S. Mohanty, Phys. Rev. **D66**, 113008 (2002), hep-ph/0203181.
- [27] J. F. Beacom and N. F. Bell, Phys. Rev. **D65**, 113009 (2002), hep-ph/0204111.
- [28] SNO Collaboration, B. Aharmim *et al.*, (2004), hep-ex/0407029.